https://doi.org/10.5194/egusphere-2025-4352
Preprint. Discussion started: 18 September 2025

New Outdoor Experimental River Facility to Study River Dynamics

Basem M. M. Mahmoud[1], Emily Dickson[2], André Renault[1], Mélanie Trudel[1], Pascale M. Biron[2], Leonard S. Sklar[2], and Jay Lacey[1]

[1]Département de génie civil et de génie du bâtiment, Université de Sherbrooke, 2500 Blvd. de l'Université,Sherbrooke, QC, CA.
[2]Department of Geography, Planning and Environment, Concordia University, 1455 De Maisonneuve Blvd. W., Montreal, QC, CA

Correspondence: Basem M. M. Mahmoud (Basem.Mohamed.Mostafa.Mahmoud@USherbrooke.ca)

Abstract.

The Outdoor Experimental River Facility (OERF) is a new large-scale, semi-natural research facility designed to study river dynamics at scales that bridge small laboratory models and natural rivers. The facility comprises a 50 m long, 20 m wide floodplain corridor and is designed to sustain discharges up to 800 $\mathrm{L\,s^{-1}}$, allowing subcritical, fully rough flow with field-like Reynolds numbers approaching 10^5—beyond values typical of small-scale planform experiments constrained by Froude similarity. In an initial 338 h (∼14 days) straight-channel run without upstream sediment feed, a bi-modal gravel–sand bed (initial $D_{50} = 10$ mm) progressively armoured to ~ 22 mm, and reach-scale planform change remained modest despite $W/D \approx 12$ and transport stage $\tau_0/\tau_c \sim 1.2$. A three-phase, mathematically designed inlet bar–pool perturbation increased local velocities by 8–27 % and produced limited lateral bank erosion (∼2.5–7.5 cm) but did not initiate meandering. The results delineate a narrow operational window for sustained bar growth and migration, long adjustment times, practical constraints of outdoor operation, and the moderating role of bank-material strength and toe armouring. Together, these findings show that field-like hydraulics are achievable within the facility while clarifying what limits mobility at this scale, and they motivate future experiments that couple hydrodynamic similarity with controlled sediment recirculation/feed and refined boundary controls to advance understanding of controls on planform evolution.

1 Introduction

Rivers shape landscapes over geologic time-scales (Wohl, 2020; Sklar, 2024) and, on human time-scales, can threaten infrastructure through erosion and flooding (Wohl, 2010; Smith, 2020). Predicting riverbank erosion and channel migration rates remains difficult, especially because planform evolution depends on many factors (Coulthard and Van De Wiel, 2012) and existing models cannot capture all relevant processes (Saadon et al., 2021; Zhao et al., 2022). A difficulty arises from the absence of robust mathematical formulations capable of capturing all the intricate processes occurring across various temporal and spatial scales (Schleiss, 2018; Rodríguez et al., 2020).

Field monitoring, physical modeling, and numerical simulation are all essential for predicting river system dynamics, yet each approach has inherent limitations. Field data can constrain river geomorphodynamic model parameters and reduce equifi-

https://doi.org/10.5194/egusphere-2025-4352
Preprint. Discussion started: 18 September 2025

nality issues, but measurements can be labour-intensive, seasonally constrained, and variable in quality (Eidmann and Gallen, 2023). Physical models enable control of key variables, but cannot reproduce the full complexity of natural river systems, particularly when extrapolating from small-scale, short-term experiments to large-scale, long-term applications (Wei and Li, 2004). Factors such as storm-driven external forcing or sediment heterogeneity, which might be negligible in a short-term flume run, become critical over longer periods. Thus, physical model results may oversimplify or neglect the influence of important factors (e.g., the erosion of cohesive banks, sediment sorting processes, or the influence of vegetation on bank stability) essential for understanding field dynamics. Numerical models, which are capable of integrating data from both field monitoring and physical models, rely on mathematical approximations and empirical relations that may misrepresent physical realities (Siviglia and Crosato, 2016; Siva Subramanian et al., 2020; Yassine et al., 2023). For instance, an empirical relation for sediment transport might work well under a narrow range of conditions but fail at different scales or with varying sediment types (Papanicolaou et al., 2008). Thus, comprehensive experimentation in diverse natural settings is needed to address these limitations, capturing the full spectrum of morphodynamic processes, including the transient and non-equilibrium behaviors (Church and Ferguson, 2015).

The majority of physical modeling experiments with erodible beds and banks are conducted at indoor small-scaled laboratory flumes (Métivier et al., 2017; Phillips et al., 2022). These models typically feature streams with depths less than 10 cm, median grain sizes (D_{50}) less than 10 mm, widths less than 1 m, and discharges on the order of 10 $\mathrm{L\ s^{-1}}$. Due to these small scales, maintaining dynamic similarity requires the relaxation of the Reynolds number, which in turn alters the fluid dynamics and can lead to hydraulic dynamics not representative of field conditions (Ashworth et al., 1996; Felder and Chanson, 2009). Additionally, excessive downscaling of sediments, especially fine particles like clay or silt, can results in unnatural patterns of sediment transport and deposition (Peakall et al., 2007). As a result, when results from small-scale flumes are up-scaled — by scale factors of 30 or more — these distortions can lead to inaccurate predictions for real-world applications (Wei and Li, 2004).

Given these limitations, large-scale experimental facilities offer the opportunity to better approximate the complexity and scale of natural river systems. By creating flow conditions at scales similar to field prototypes, large facilities can create realistic Reynolds numbers and turbulent structures, expand the range of experimental variables, and provide more accurate representations of natural conditions. However, working at larger scales still requires a balance between realism and control (Kakinuma and Shimizu, 2014).

Despite the importance of large-scale experimentation, only a few large-scale experimental channels exist. The Outdoor StreamLab (OSL) at the St. Anthony Falls Laboratory (SAFL) in Minnesota, USA, offers a 40 by 20 meter basin with a meandering sand-bed stream, enabling for example detailed studies of sediment transport and flow-vegetation interactions under controlled yet field-like conditions (UMN-CSE, 2023; Métivier et al., 2016). The River Experiment Center (REC) at the Korea Institute of Civil Engineering and Building Technology (KICT) in Andong, South Korea, features three prototype channels, each approximately 600 meters long, facilitating large-scale experiments on flow patterns, sediment transport, and hydraulic structure stability (KICT, 2023; Han et al., 2019). The Aqua Restoration Research Center (ARRC) in Kakamigahara City, Japan, includes three 800 meter long experimental streams designed to simulate natural river conditions (PWRI-NRDA,

https://doi.org/10.5194/egusphere-2025-4352
Preprint. Discussion started: 18 September 2025

2023). Together, these facilities have advanced our understanding of rivers, producing more than 50 publications on a range of topics, as illustrated in Figure 1, yet none of them permit dynamic evolution of river planform on a reach scale. Therefore, expanding and diversifying experimental facilities is crucial to accurately capture the full spectrum of river behaviors.

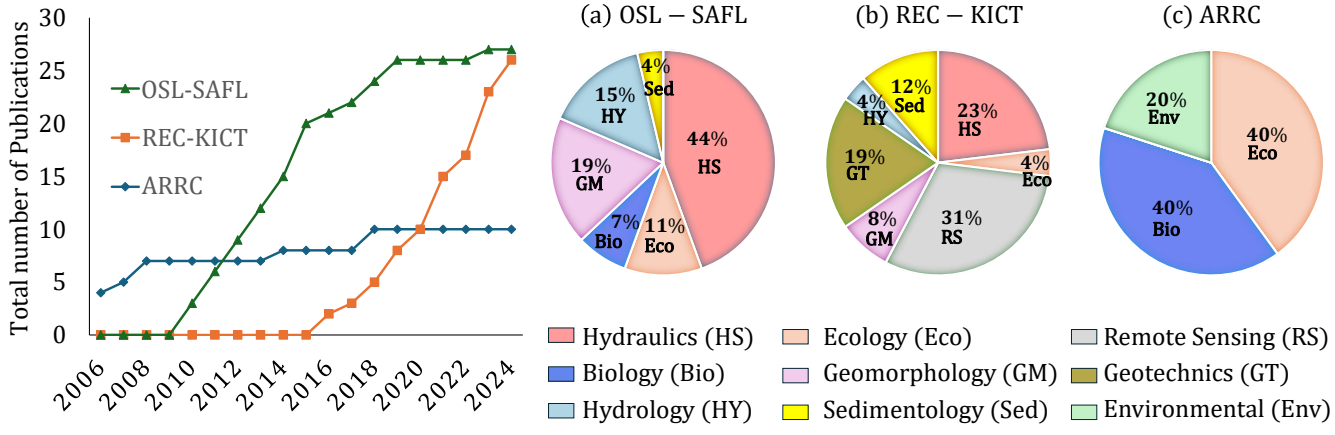

Figure 1. Number of publications from the large-scaled outdoor experimental facilities with categorized research fields contributions. Only English language articles published in journals with an impact factor greater than 1.5 according to the 2024 Clarivate Journal Citation Report are included.

At the Université de Sherbrooke, in Quebec, Canada, a large-scale river facility known as the Outdoor Experimental River Facility (OERF) has recently been constructed to help bridge the gap between field and laboratory-scale studies. This facility combines the features of large-scale facilities with the capacity for erodible banks, allowing for natural processes of bank erosion and planform evolution to occur. The OERF's monitored and controlled environment provides opportunities to test theories previously validated through small-scale flume experimentation to determine if theoretical predictions are also valid at field scales (Wilcock and Crowe, 2003). In this paper we: (1) introduce the design and capabilities of the OERF, and compare it to natural rivers and other facilities; (2) report the results of initial experiments in a straight channel configuration, including the effects of a novel bar perturbation; and (3) evaluate these results to illustrate opportunities and constraints of working at large scale. We frame the study around four themes relevant to large-scale experimentation: (i) the narrow operational window in parameter space for sustained bar building and lateral migration; (ii) the longer adjustment timescales of a large system and the transient evolution away from initial conditions; (iii) the challenges of an outdoor setting (e.g., seasonal algal growth, rainfall, wildlife); and (iv) the importance of bank-material strength and toe armouring for erosion. In our initial test runs, the flow in the OERF channel achieved hydrodynamic similarity at field-like Reynolds numbers. However, without sediment supply, the bed armoured, planform adjustment remained limited, and bank erosion was localized at the perturbation.

https://doi.org/10.5194/egusphere-2025-4352
Preprint. Discussion started: 18 September 2025

2 Facility design and capabilities

2.1 Facility components

The OERF (Outdoor Experimental River Facility) is composed of four primary components: a main reservoir, an approach channel, a river-floodplain basin (50 m long and 20 m wide), and a sediment trap (Figure 2). The OERF recirculating system stores up to 1500 m^3 of water. Water is pumped from the main reservoir to the approach channel, which is designed to dissipate energy and reduce turbulence before the flow enters the river floodplain. A sharp-crested weir is situated at the transition between the approach channel and the floodplain, which can be used to measure flow. Once the water passes through the river floodplain, it flows into the main sediment trap before returning to the main reservoir.

The water circulation at the OERF is controlled from a pump house, with remote operation capabilities via a local WiFi network and emergency stop buttons located near the floodplain for safety. The water system is driven by two variable-speed 100 hp centrifugal pumps, which together can deliver a maximum flow rate of approximately 800 $\mathrm{L\ s^{-1}}$. The facility includes a dedicated bay for a third identical pump, enabling a future increase in capacity to about 1,200 $\mathrm{L\ s^{-1}}$ without major civil works.

To maintain hydraulic equilibrium and prevent groundwater exchange, the reservoir, approach channel, and river region are lined with an impermeable geomembrane. In the river floodplain corridor, the membrane is buried beneath a substrate layer at least 1 meter thick, which is composed of silt, sand, and gravel. The experimental corridor can accommodate various river geometries based on experimental designs and objectives. The corridor substrate and surface grain-size distribution are specified on a per-experiment basis.

The facility is designed to accommodate sediment transport experiments with and without external sediment feed. During the preliminary tests reported here, no sediment was fed or recirculated. A dedicated sediment-recirculation system has been constructed to enable controlled reintroduction of a sediment–water mixture pumped from a smaller downstream sediment trap to the upstream inlet. The system employs a 6 inch eductor (Model FFTLS14-6-D, Elmridge Jet Apparatus) driven by a secondary motive pump (20 hp); the eductor uses differential pressure to entrain sediment and water via a vertically oriented 3 inch suction pipe. The recirculation loop is provisioned for instrumentation with manometers on the motive and suction lines and a flowmeter unit at the discharge line. This system was under construction during the initial experiments presented in this article.

2.2 Data acquisition capabilities

The OERF is designed to allow the floodplain corridor to drain completely when the pumps are stopped, facilitating rapid and efficient data collection. Topographic data are acquired using multirotor UAVs capable of RGB photogrammetry (e.g., DJI Matrice 300 series), multispectral imaging (e.g., DJI Mavic 3 Multispectral), and LiDAR (e.g., Zenmuse L2). Ground-based elevation control and survey are obtained with GNSS-RTK receivers (e.g., Leica GS18) and a robotic total station (e.g., Leica Viva TS15); laser levels are used for rapid local elevation checks, slope adjustments, and instrument setup.

Hydrometric measurements are supported by pressure transducers for stage monitoring. Flow velocities within the channel are measured using either large-scale particle image velocimetry (LSPIV) from UAV video, electromagnetic current meters

https://doi.org/10.5194/egusphere-2025-4352
Preprint. Discussion started: 18 September 2025

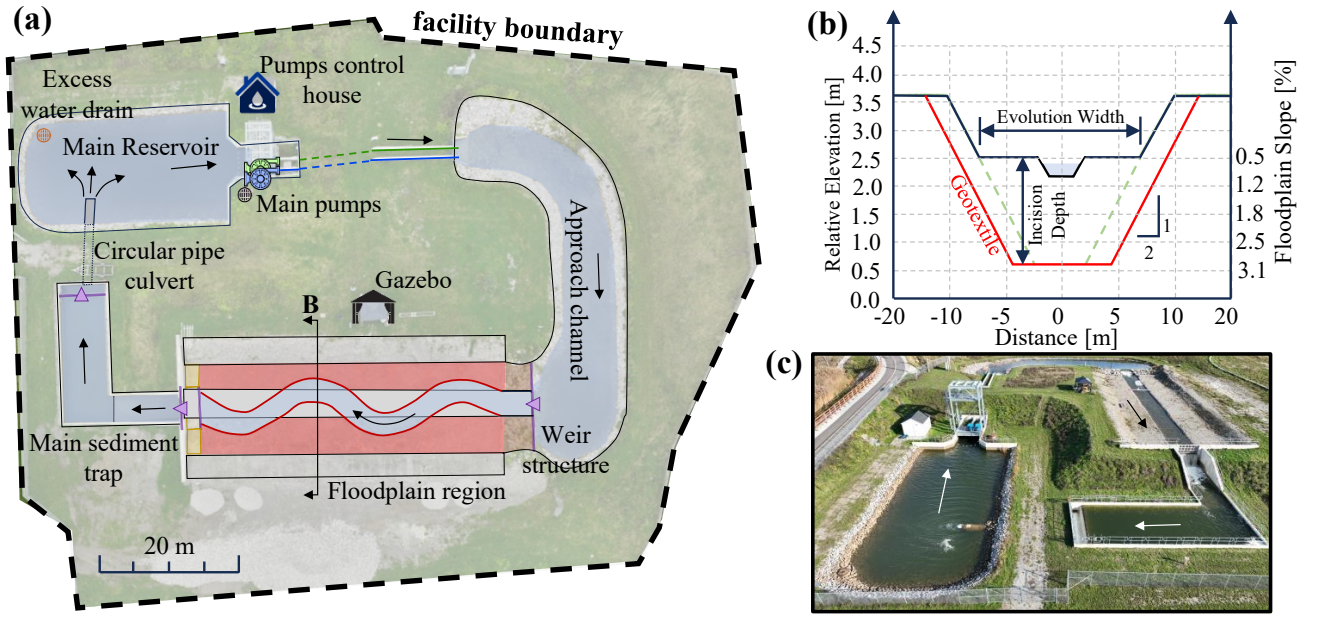

Figure 2. The Outdoor Experimental River Facility Components. (a) Plan view, (b) Distorted cross-section in the floodplain at 20 m upstream the river outlet, the potential evolution width and incision depth vary with floodplain slope shown on the secondary (right) y-axis. Green dashed lines extend the design corridor side-slope, while the red line marks the geotextile boundary. (c) Oblique aerial drone photo of the facility.

(ECM), acoustic Doppler velocimeters (ADV), or propeller-type current meters. Sediment-transport sampling infrastructure includes portable bedload samplers (e.g., Helley–Smith) and bedload traps (e.g., Bunte-type) deployable at selected cross-sections.

2.3 Comparison with natural rivers and existing facilities

As a large-scale outdoor facility, the OERF is situated between typical indoor laboratory channels and natural rivers. The green shading in Figure 3 shows a design envelope of feasible combinations of discharge, slope, median grain size, and channel width that can be configured within the facility limits. These combinations were computed from standard open-channel hydraulic relations, assuming a rectangular cross-section and normal depth (MATLAB code in the supplements).

Within this parameter space, researchers can use the OERF to work at meter-scale widths while maintaining field-like hydraulic similarity. Typical combinations yield turbulent, subcritical flows with Reynolds numbers clustered around $Re \sim 10^5$ and Froude numbers near $Fr \approx 0.6$. These values overlap the low-width corner of the natural-river data compilation ($Re \approx 10^6$) and extend beyond most indoor facilities ($Re \approx 10^3$) while keeping $Fr < 1$ over most of the envelope. Scaling to larger

https://doi.org/10.5194/egusphere-2025-4352
Preprint. Discussion started: 18 September 2025

rivers with $Re \gtrsim 10^6$ would still require some relaxation of Reynolds similarity, but the present regime preserves the essential turbulent character at widths (0.2–5 m) and grain sizes (D_{50} = 2–100 mm).

Practical constraints make the current operational window narrower than the theoretical envelope. Pump capacity ($Q_{max} \approx 800\ \mathrm{L/s^{-1}}$), slope $< 3\%$, depth < 0.5 m, and available sediment sources limit D_{50} given the attainable combinations of velocity and depth. Outdoor operation adds expense, variability (e.g., algal growth, rainfall), and bank properties (roughness, strength) are more difficult to control than in a smaller indoor flume. Consequently, only a subset of parameter combinations is currenlty practical for sustained runs.

Even with these constraints, the envelope reaches dimensionless regimes associated with bar formation and planform dynamics. Width-to-depth ratios span from single digits to $\mathcal{O}(10^2)$ (median ≈ 16, max ≈ 221), and maximum bankfull Shields numbers approaching ≈ 1.45 at D_{50} of 2 mm. Thus, there exists a parameter space where the OERF can be configured to probe questions that depend on secondary currents, bank stresses, and mobility while sustaining a field-like Reynolds similarity.

3 Initial experiments at the OERF

3.1 Design of initial experiments

To test the operation and capabilities of the OERF, we conducted a series of preliminary experiments. Detailed descriptions of the design and results of the initial experiments are available in the MSc thesis of Dickson (2023). These initial runs were designed to explore thresholds in channel planform evolution without inlet sediment supply. We focused in particular on whether a straight channel would develop incipient meandering in response to a perturbation in the bed topography. A 90 h conditioning run (Phase 0 in Table 2) preceded the imposed perturbation to allow water-working of placed sediments to allow the bed to adjust to initial hydraulic conditions. Subsequent phases introduced a controlled bar–pool perturbation near the inlet (Sect. 3.2) in three height increments to evaluate whether a localized topographic impulse could trigger development of alternate bars and lateral migration under sediment-limited conditions.

Operating conditions (Table 1) included: steady discharge (Q) = 720 $\mathrm{L\,s^{-1}}$, bed slope (S) = 0.005, trapezoidal cross-section geometry (2H:1V), bottom width (W) =2.5 m, and median surface grain size (D_{50}) =10 mm). These choices yield subcritical, fully rough flow ($Fr \approx 0.63$; $Re \approx 2 \times 10^5$) at width–to–depth $W/D \approx 12$, placing the experiment within the OERF envelope where turbulent similarity is preserved at meter scale while remaining practical to operate (Figure 3).

The initial bed and banks were composed of the floodplain material placed over the geomembrane, featuring a bi-modal grain-size distribution (GSD) of coarse gravel and sand (Figure 4). The sediment composition includes approximately 50% gravel, 46% sand, and 4% of fines, with particle sizes ranging from less than 0.08 mm to 112 mm, which corresponds to a poorly sorted GSD according to Folk and Ward (1957), with a Sorting Coefficient of 1.2.

The experimental channel conditions were designed to generate an average transport stage (i.e. ratio of Shields parameter to a critical value of 0.045) greater than 1.2. Under these initial conditions (Table 1) more than 60% of the initial GSD was predicted to be transported as bedload, with a transport capacity of up to 50 $\mathrm{kg\ min^{-1}}$ using the surface-based predictor of Wilcock and Crowe (2003) (Figure 4).

https://doi.org/10.5194/egusphere-2025-4352
Preprint. Discussion started: 18 September 2025

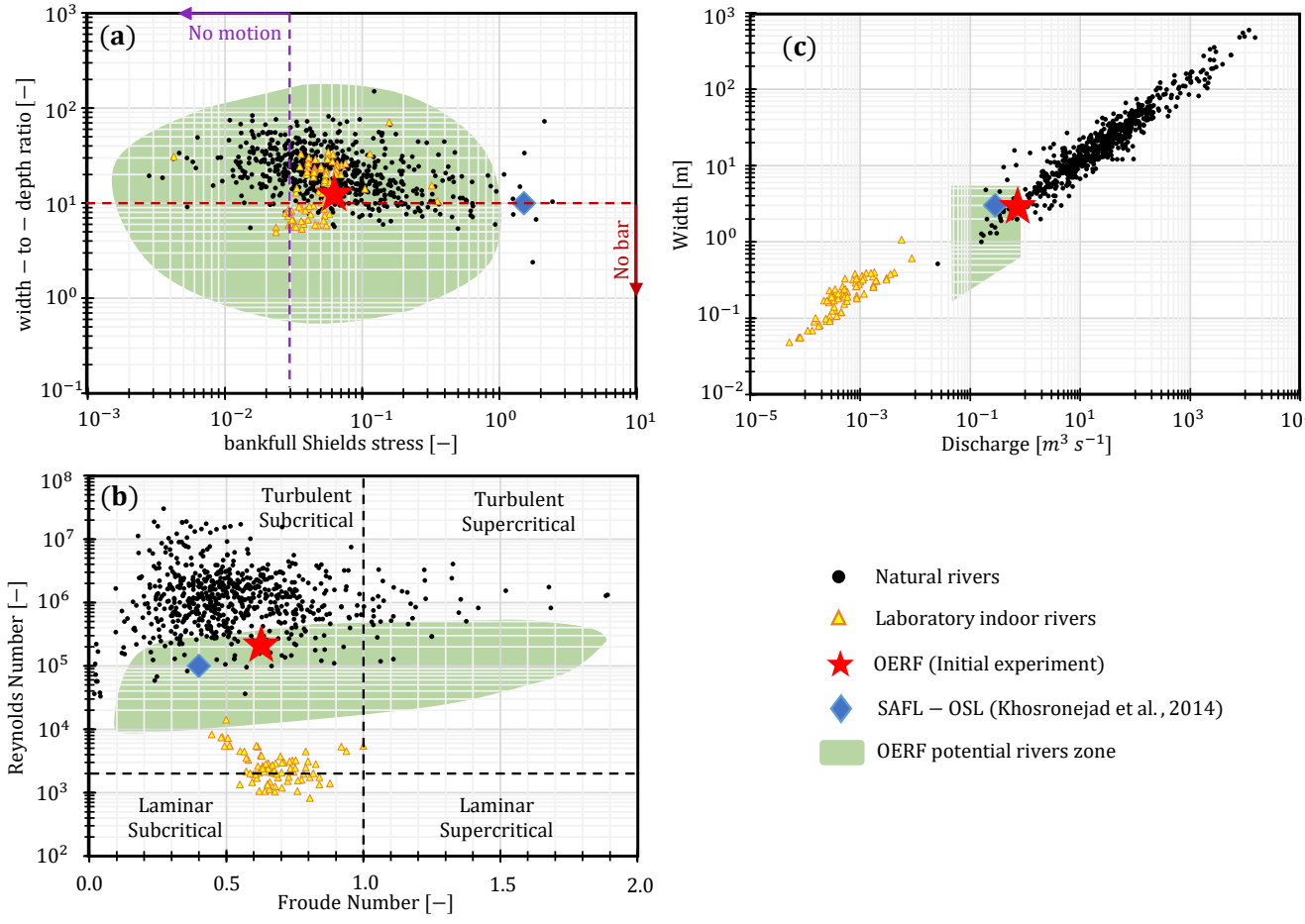

Figure 3. OERF in comparison with other experimental facilities and natural rivers. (a) width–to–depth ratio vs. bankfull Shields number, $\theta = \tau_0/[(\rho_s - \rho)gD_{50}]$; No-motion guide line at $\theta_c = 0.03$ for D_{50}, representing the lower bound of visually defined incipient-motion thresholds in gravel-bed rivers (Buffington and Montgomery, 1997); No-bar guide line at $W/D = 10$, below which free (periodic) alternate bars are not expected (Crosato and Mosselman, 2020). (b) Reynolds vs. Froude number with schematic regime quadrants. (c) width vs. discharge. The green shaded area marks the range of OERF potential channels, constrained by current facility limits: discharge 50–800 L s^{-1}, slope 0.1–3 %, median grain size D_{50} = 2–100 mm, channel width 0.2–5 m, and flow depth < 0.5 m. The envelope represents feasible design combinations; extreme bounds may not be possible simultaneously. Natural rivers dataset from Phillips et al. (2022), filtered to include only sand-bedded and gravel bed rivers. Laboratory indoor rivers from Métivier et al. (2017). St. Anthony Falls Laboratory (SAFL) - Outdoor StreamLab (OSL) from Khosronejad et al. (2014).

3.2 Inlet perturbation design

155 Previous experimental studies have used controlled perturbations to initiate bars and, in some cases, meandering. In a simple configuration, Braudrick et al. (2009) aligned the entrance channel at a small angle to a downstream straight reach, creating

https://doi.org/10.5194/egusphere-2025-4352
Preprint. Discussion started: 18 September 2025

Table 1. Initial experimental river conditions at the OERF.

Parameter	Value
Bankfull discharge	$720\ \mathrm{L\,s^{-1}}$
Bed slope	0.005
Geometry (side slope)	Trapezoidal (2H:1V)
Bottom width	$2.5\ \mathrm{m}$
Median grain size, D_{50}	$10\ \mathrm{mm}$
Average depth	$0.25\ \mathrm{m}$
Froude number, Fr	0.63
Reynolds number, Re	2×10^5

Table 2. Experimental duration by phase.

Phase	Description	Total (h)
0	Armouring / no bar	90
1	One-third bar height	15
2	Two-thirds bar height	28
3	Full bar height	205

a bend that seeded flow vorticity, bank erosion, and meander growth. Building on this idea, Van Dijk et al. (2012) used a transversely movable inlet to impose time-varying planform forcing and accelerate meandering. In straight channels, other work has promoted alternate-bar development by partially blocking the upstream entrance (Nelson et al., 2010). Here, we used a constructed bar–pool unit near the inlet to perturb the flow with the goal of catalyzing alternative bar development, bank erosion and meander growth.

We designed the bar–pool unit following the morphometric framework of Redolfi et al. (2020) and Froude-similitude outlined by Parker et al. (2003) (Figure 5). To ensure morphological consistency, the scaling factor was determined by identifying the discharge in the Redolfi et al. (2020) experiments that produced a width-to-depth ratio comparable to that of the present study. This condition was met at a discharge of $2.5\ \mathrm{L\ s^{-1}}$ in their flume experiments. Based on this reference case, we adopted a scaling factor of 10, consistent with scaling ratios derived for discharge, channel width, and median grain size. Accordingly, the dimensions of the perturbation structure were scaled to $230\ \mathrm{mm}$ in height, $43\ \mathrm{mm}$ in relief, and $21\ \mathrm{m}$ in wavelength. Relief is defined as the standard deviation of detrended bed elevations within the bar unit, which is about one-fifth of the maximum bar height (Figure 5).

https://doi.org/10.5194/egusphere-2025-4352
Preprint. Discussion started: 18 September 2025

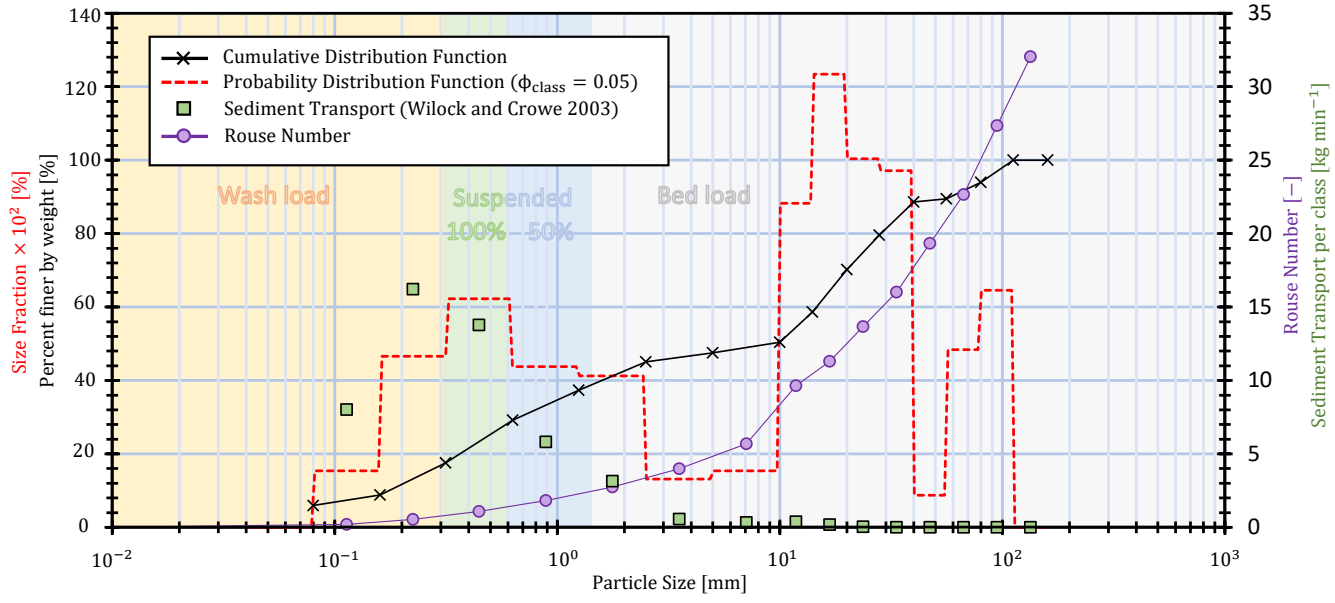

Figure 4. OERF grain size and sediment transport characteristics in preliminary experiments based on the physical parameters outlined in Table 1. The cumulative distribution function (black line) and the probability distribution function (red dashed line, binned by log transformed grain size$\phi_{\text{class}} = 0.5$, values multiplied by 10^2 for clarity) are read on the primary y-axis at left. The Rouse number (purple line with circles), computed following Borsje et al. (2014) using the fall-velocity expression of Ferguson and Church (2004), together with the sediment-transport rate per grain-size class predicted by the Wilcock and Crowe (2003) formula (green squares), are read on the secondary y-axis at right. Background shading denotes transport regimes (wash load, suspended load, bed load) corresponding to Rouse-number thresholds.

To generate the perturbation topography, Fourier components (harmonics) were applied as $\eta(x, y) = \sum_{n,m} |A_{nm}| \cos(\pi m y/W) \cos\left(2\pi n x/L + \phi_{nm}\right)$, with amplitudes ($A_{nm}$) and phases ($\phi_{nm}$), for longitudinal ($n$) and transverse ($m$) modes tuned to reproduce a realistic bar-pool asymmetry (Figure 5). A sensitivity analysis of these harmonics can be explored at math3d.org/NJYVGn2Eg.

We only constructed the upstream half of the unit to explore whether subsequent erosion and deposition would extend the bar-pool morphology downstream. The bar was made with non-erodible (sandbags filled with < 10 mm sediment) to preserve geometry between phases; the adjacent pool was excavated into the bed substrate to maintain cross-sectional area as bar height increased through three steps (Table 2). We positioned the perturbation near the inlet to maximize its hydraulic influence and the usable experimental length downstream. We allocated approximately 4.45 m of upstream channel length for post-cascade energy dissipation and an additional 4.0 m for flow development (Figure 5).

3.3 Rationale and hypothesis for experimental design

Meandering initiation thresholds and planform adjustment pathways have been documented previously for gravel-bed channels (Knighton, 2014; Rhoads and Welford, 1991; Rhoads, 2020). Straight channel configurations are inherently unstable, and

https://doi.org/10.5194/egusphere-2025-4352
Preprint. Discussion started: 18 September 2025

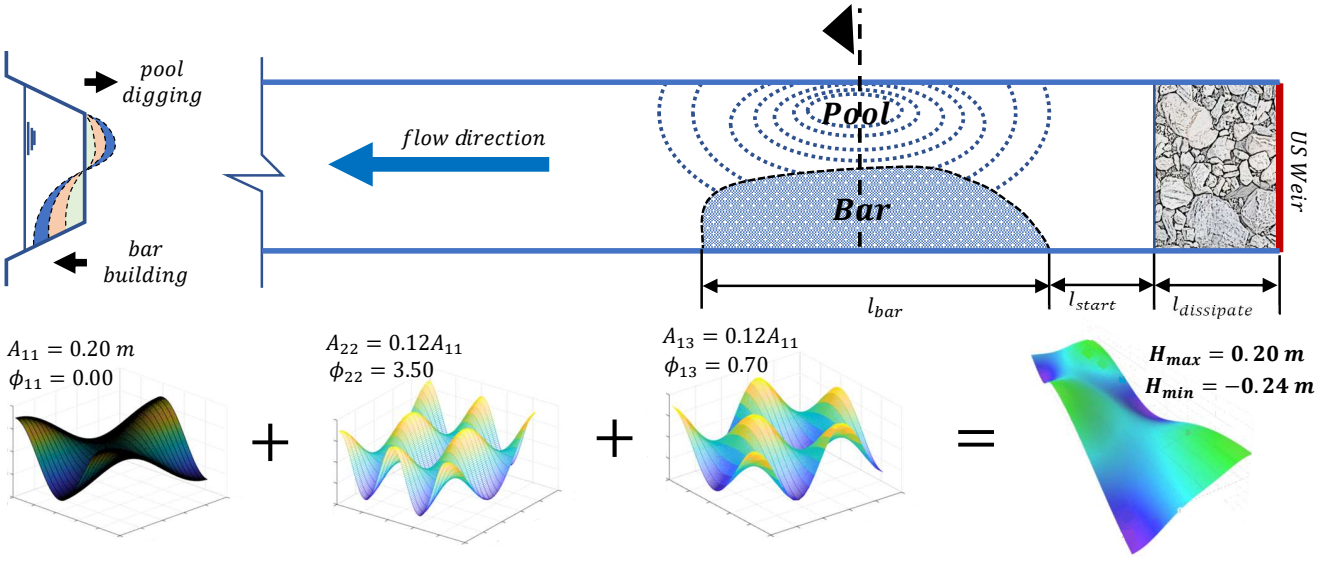

Figure 5. Schematic of the inlet perturbation location with harmonics superposition

under a range of conditions should evolve into a meandering pattern through stages as described by Knighton (2014). Initially, bedform development (Stage 1) leads to the formation of alternating bars that concentrate flow and drive bed erosion (Rhoads and Welford, 1991). Subsequently, the formation of pools and cross-over riffles (Stages 2 and 3) amplify bank erosion and accelerate bend formation (Rhoads, 2020), ultimately resulting in increased sinuosity characterized by riffles at inflection points and pools at bend apexes. Laboratory studies have demonstrated that inlet perturbations or geometric asymmetries can seed this sequence of planform evolution (Braudrick et al., 2009; Van Dijk et al., 2012).

In designing our initial experiments in the OERF, we hypothesized that under steady discharge and in the absence of upstream sediment supply, meandering could still develop due to entrainment of sediment supplied by bank erosion leading to downstream bar development. In particular, we hypothesized that a localized bar–pool perturbation would concentrate shear stress near the outer bank, enhance secondary circulation, and trigger initial bend growth via bank erosion, pool scour, and downstream deposition of eroded material into bars. The null hypothesis was that the armoured channel bed would remain stable, inhibiting sediment transport and morphological evolution over the time scale of the experiment.

3.4 Measurements and data processing

High-resolution topography was acquired at the end of each of the four phases using multirotor UAV imagery for structure-from-motion (SfM) photogrammetry with 80% forward and side overlap at a flight altitude of 10 m. Flights used a DJI Mavic 2 Pro; when that drone was unavailable, a DJI Mini 2 was used, which increased DEM noise relative to the Mavic 2 Pro. Ground control points (GCPs) were established with a Leica Viva TS15 total station set with benchmarks that had been established by GNSS-RTK. Each flight was georeferenced using a minimum of 6 and a maximum of 12 GCPs. Images were processed in

https://doi.org/10.5194/egusphere-2025-4352
Preprint. Discussion started: 18 September 2025

Pix4Dmapper with phase DEMs and orthomosaics were exported at a 2 mm grid resolution. DEMs of Difference (DoD) were then computed in ArcGIS between phases to map erosion and deposition within the corridor applying a minimum detectable change threshold of 2.5 cm.

To track bed-surface coarsening, nadir photographs were acquired at fixed locations using a smartphone held approximately 90° to the bed. Each image covered a $1.0\ \mathrm{m} \times 0.70\ \mathrm{m}$ patch and included a metric ruler for scale. Images were imported to AutoCAD (2D) and scaled by matching the photographed ruler length. A 5 cm mesh grid was overlaid and a grid-by-number sampling was performed (Bunte and Abt, 2001). The b-axis was digitized as a polyline, yielding about 275 pebble measurements per patch. Surface size distributions were computed from the empirical cumulative distribution of the measured b-axes.

Velocity profiles were collected with a side-looking acoustic Doppler velocimeter (ADV) mounted on a rigid traverse. The measurement cross-section was located at the bar apex. A fixed sampling grid was used: near-bank rows were 2.5, 5.0, 7.5, 10, 15, and 20 cm above the bed with lateral offsets of 2.5, 5.0, 7.5, 10, 15, and 20 cm from the bank; mid-channel columns were 100, 140, and 180 cm from the bank with vertical offsets of 2.5, 4.0, 6.0, 10, and 15 cm above the bed. At each point the ADV sampled at 50 Hz for 120 s using a $\sim 1\ \mathrm{cm}^3$ sampling volume.

Shear velocity u_* was estimated by fitting the time-averaged vertical profiles to the logarithmic law $u(y) = u_*/\kappa \ln\big(y/y_0\big)$ with $\kappa = 0.41$ (Biron et al., 2004; Dey, 2014). Fits were restricted to heights outside near-bed interference and within the presumed log-layer; because many sampling heights in these runs lay above the inner $\sim 20\%$ of depth, the resulting u_* estimates carry additional uncertainty; profiles lacking a coherent log-region were discarded (Afzalimehr and Anctil, 1999). Bed shear stress was computed as $\tau_0 = \rho u_*^2$. The Shields number $\theta = \tau_0/[(\rho_s - \rho)gD_{50}]$ is reported using the phase-specific surface D_{50} (initial 10 mm, ≈ 17 mm after Phase 0, ≈ 22 mm after Phase 3). For reference, the critical stress was estimated as $\tau_c = (\rho_s - \rho)g\theta_c D_{50}$ with $\theta_c = 0.045$, i.e. $\tau_c \approx 728\, D_{50}$ (with D_{50} in metres, τ_c in Pa).

Water depth was recorded with a submerged pressure transducer (Solinst Levelogger) installed at mid–reach to track steady discharge conditions and changes in depth. Atmospheric pressure was removed by barometric compensation using a co-located barometer. Sensors experienced episodic fouling by filamentous algae (see examples in Dickson (2023)); which was periodically cleaned to maintain data quality.

Bank retreat adjacent to the perturbation was quantified between phases using cross-sectional geometry rather than planform banklines to capture changes in bank topography. For each phase, we extracted elevation profiles from the DEMs (at the same location as the ADV section) and measured the horizontal shift of the bank side-slope due to erosion including undercutting.

4 Results and Discussion

4.1 Physical responses of the OERF

Over the initial 90 h conditioning run, the channel was allowed to freely evolve from the original straight channel configuration under constant flow conditions and no external sediment supply. Only limited morphological change was observed during this

https://doi.org/10.5194/egusphere-2025-4352
Preprint. Discussion started: 18 September 2025

period, with the channel remaining predominantly straight. Minor bed elevation fluctuations of about ± 2 cm occurred near the outlet, likely due to backwater effects, and a coarse surface layer developed on the bed (Figure 6A).

During this initial rum, an armouring process gradually became dominant. Approximately 40% of the initial fine-grained sediment was removed as suspended load, leaving behind larger gravel particles (>10 mm) that exhibited transport rates below 1 kg min^{-1} (Figure 4). Consequently, the median grain size (D_{50}) increased from 10 mm to 17 mm, and then to 22 mm post phase 3, reflecting continuous bed coarsening (Figure 6C). Visual inspection revealed a transition from matrix to clast-supported bed structure over the experiment (Figure 6B). The stable armour layer reduced channel erodibility, limiting morphological evolution and increasing lateral channel stability (Rachelly et al., 2022). These armouring dynamics are consistent with patterns observed in natural gravel-bed rivers subjected to reduced sediment supply (Dietrich et al., 1989; Chin et al., 1994) and align with laboratory flume findings reported by Elgueta-Astaburuaga and Hassan (2017). Depth measurements show that as armouring developed, flow depths stabilized, demonstrating the linkage between bed texture and hydraulic conditions (Figure 6D). Detailed information and results of additional numerical modeling of the armouring process are available in the MSc thesis of Renault (2024).

Following the conditioning run, an bar-pool perturbation was introduced to accelerate morphodynamic adjustments and potential meandering. The perturbation, in three incremental phases, progressively influenced local flow dynamics and channel morphology (Figure 7A). During Phase 1 (bar at 1/3 height), minor bank erosion occurred on the right bank adjacent to the perturbation, with lateral erosion ranging between 2.5 and 5 cm. Phase 2 (bar at 2/3 height) resulted in more pronounced erosion, extending approximately 2 meters downstream with maximum erosion reaching about 7.5 cm. By Phase 3 (full bar height), erosion further expanded approximately 4 meters downstream on the right bank opposite the perturbation, with lateral erosion ranging from 2.5 to 5 cm. Notable erosion was also observed on the left bank, beginning approximately 6 meters downstream of the perturbation and extending approximately 8 meters further downstream, with erosion between 2.5 and 7.5 cm. Cross-sectional profiles shown in Figure 7C detail the progressive deformation of the bank through these phases. This limited cross-sectional evolution reflects high bank-material strength due to the stabilizing influence of the coarse tail of the grain size distribution and armouring at the toe of the bank. Bank cohesion, particularly in the upper portion of the bank above the water line, also contributed to limiting lateral adjustment.

Despite these local responses, reach-scale morphology remained largely straight over the experiment duration. Together with the absence of upstream sediment supply and the conditioned, armoured bed, these observations indicate that planform adjustments were modest under the explored combinations of discharge, grain size, and bank strength within the experiment timescale.

4.2 Flow structure, velocities, and shear stress

The impact of the bar perturbations on velocity distribution and bed shear stress was investigated using a side-looking ADV indicated in Figure 8 and Figure 9. Velocity and shear stress patterns show a localized intensification of boundary forcing near the perturbation.

https://doi.org/10.5194/egusphere-2025-4352
Preprint. Discussion started: 18 September 2025

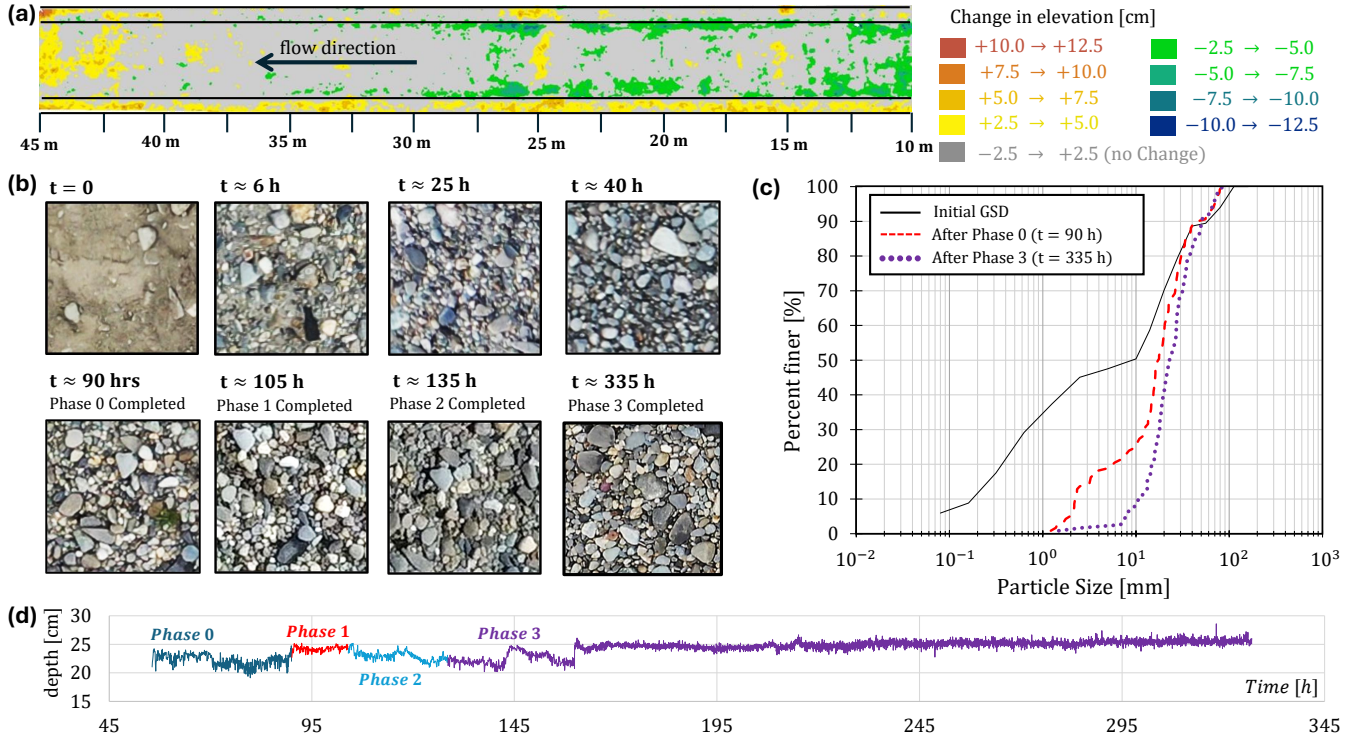

Figure 6. Physical response of armouring processes. (a) Topographic change after phase 0 ($t = 90\ h$) with elevation change classified by colour scale (in cm). (b) Texture evolution of surface composition across the four phases in a 50 cm × 50 cm frame at midstream (40 m from upstream). (c) GSD: initial (Volume-by-weight), and post-Phase 0 and Phase 3 (digitally sieved, grid-by-number). (d) Flow depth at midstream (longitudinally and transversely) over the four phases.

Peak streamwise velocities in the upstream zone rose from 1.38 $\mathrm{m\,s^{-1}}$ (Phase 0) to 1.49 $\mathrm{m\,s^{-1}}$ (Phase 1), an increase of about 8%. Subsequent phases showed further increases to 1.56 $\mathrm{m\,s^{-1}}$ (Phase 2) and 1.75 $\mathrm{m\,s^{-1}}$ (Phase 3), about 13% and 27% above Phase 0. Mean streamwise velocities initially decreased slightly, from 0.88 $\mathrm{m\,s^{-1}}$ in Phase 0 to 0.84 $\mathrm{m\,s^{-1}}$ in Phase 1, then increased to 0.90 $\mathrm{m\,s^{-1}}$ (Phase 2) and 1.07 $\mathrm{m\,s^{-1}}$ (Phase 3) (Figure 8). The core region of maximum velocity shifted toward the right bank as the bar grew and the adjacent pool deepened, indicating lateral deflection and redistribution of high-velocity flow induced by the perturbation. Each phase combined an increase in bar height (non-erodible sandbags) with excavation of an erodible pool to maintain cross-sectional area. In Phase 1 the pool excavation effect was sufficiently pronounced to counterbalance the small bar relief, explaining the temporary drop in mean velocity despite a higher peak.

Bed shear stress was quantified at the perturbation cross-section using log-law method. Phase-median stresses were $\tau_0 \approx 10, 16, 29$, and 20 Pa for Phases 0–3, respectively, corresponding to median Shields numbers $\theta \approx 0.06, 0.10, 0.18$, and 0.12. For reference, phase-specific critical stresses based on the mid-reach surface D_{50} (not the local bed at the perturbation) were $\tau_c \approx 7, 12, 15$, and 16 Pa. Thus, τ_0 exceeded τ_c from Phase 1 onward and peaked in Phase 2, coincident with the strongest

https://doi.org/10.5194/egusphere-2025-4352
Preprint. Discussion started: 18 September 2025

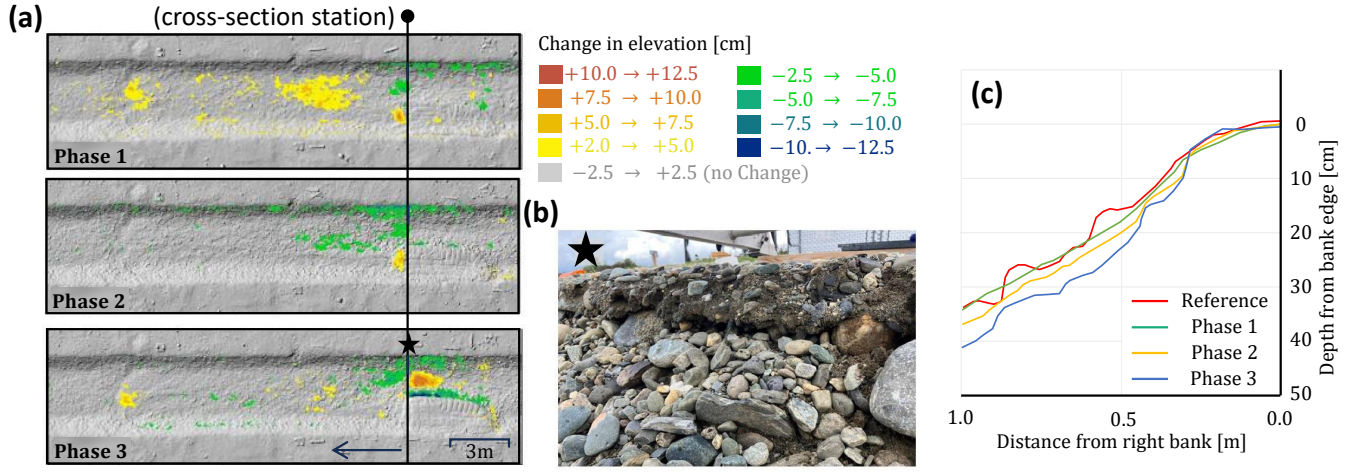

Figure 7. Physical response to the inlet perturbation. (a) Topographic changes over Phases 1–3, highlighting zones of erosion and deposition relative to the pre-perturbation reference. The black vertical line marks the location of the cross-section shown in (c). (b) Field image of the eroded right bank post phase 3 taken at the apex of the bar and the location of maximum pool scour identified on (a) with a black star. (c) Cross-sectional elevation profiles at the right bank, extracted at the location shown in (a), showing progressive erosion across phases.

observed local bank retreat. The decrease in median τ_0 in Phase 3, despite higher peak velocities, is consistent with momentum redistribution as the pool deepened and with growth of a coarse near-bank surface that limited effective shear at the log-layer fitting heights.

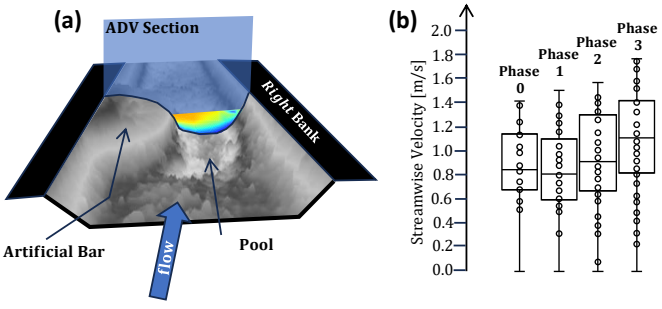

Figure 8. (a) Schematic perspective of the artificial perturbation at full form, showing the location of the ADV cross-section (blue overlay). (b) Boxplots of the streamwise velocity component (u, in $\mathrm{m\,s^{-1}}$) for each phase. Each box aggregates all time-averaged values from the ADV measurement points. These data represent the distribution of u across space (all points) and over time (averaged per point), describing the statistical evolution of streamwise flow velocity in response to progressive bar-pool perturbation.

https://doi.org/10.5194/egusphere-2025-4352
Preprint. Discussion started: 18 September 2025

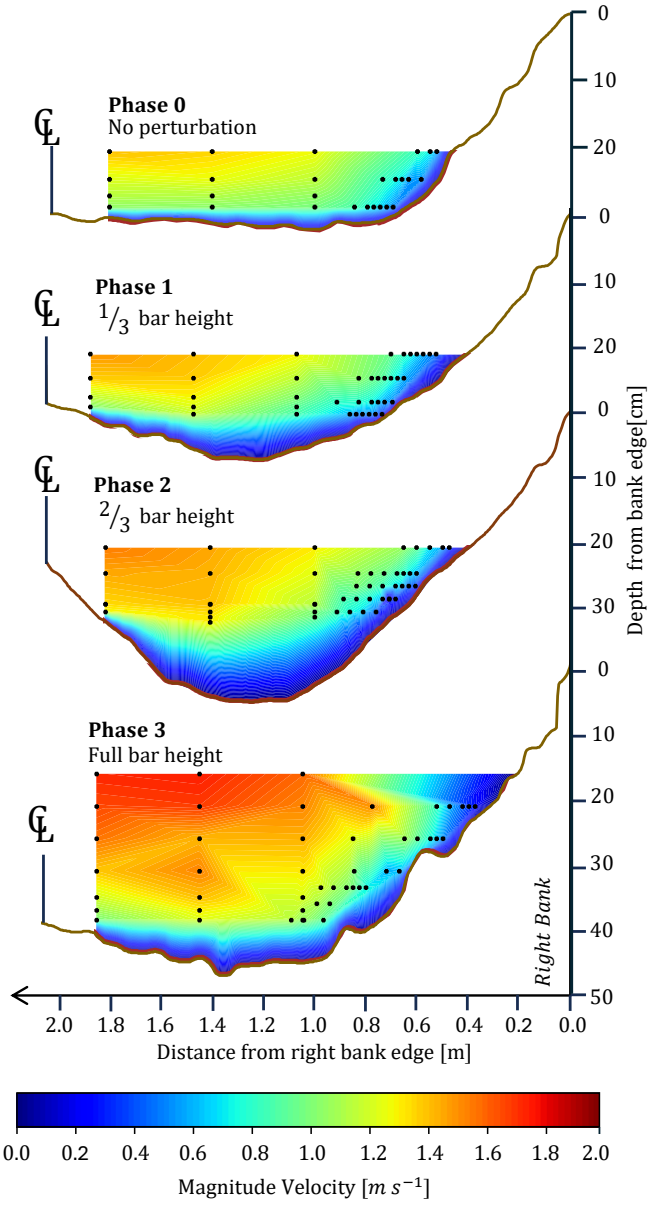

Figure 9. Time-averaged velocity magnitude fields for Phases 0, 1, 2, and 3 at the bar apex in $\mathrm{m\ s^{-1}}$. Black dots indicate ADV measurement locations. The topographic profile represents the surveyed cross-section at the end of each Phase.

4.3 Lessons learned

Several lessons emerged during the preliminary experimental phase at the OERF, many of which stem from the inherent challenges with large-scale, outdoor flume experiments. Each constraint points to practical refinements for future experiments.

https://doi.org/10.5194/egusphere-2025-4352
Preprint. Discussion started: 18 September 2025

Achieving measurable bend growth at this scale requires tuning sediment mobility and bank forcing to the feasible experimental run time while preserving channel form. To shift from a straight channel to a self-maintained meandering planform, without overshooting into braiding, future experiments should couple stronger bank-erosion drivers (e.g., higher stream power, steeper slope, greater sediment load) with sufficient bank strength (e.g. vegetation) to maintain width–to–depth ratios within the meandering domain ($W/D \lesssim 50$; Fredsøe, 1978). With the current conditions of the OERF, particles coarser than ~ 30 mm remained immobile at the available shear stresses and tended to cluster, locally locking parts of the bed and banks; for future experiments, sieving the bed sediment mixture to limit the coarse tail to ~ 30 mm is recommended.

For future experiments in the OERF exploring controls on bank erosion and lateral migration, we recommend: (i) activating the sediment-recirculation system, (ii) developing capacity to feed the recirculation system with additional sediment to widen the range of possible sediment supply, (iii) extending run duration from days to weeks, and (iv) tuning operating combinations (slope, sediment distribution, width) to accelerate expected morphological response rates to maximize the available experimental time window. In addition, to accelerate planform evolution, we suggest creating an initially sinuous channel planform and exploring the influence of discharge variability. Other physical improvements to the OERF should include a flow-straightening diffuser below the entrance cascade to reduce turbulence intensity at the inlet and a PID-controlled tail-gate weir to reduce downstream backwater effects.

Measuring shear stress in the OERF channel remains challenging due to the roughness of the bed and banks (Biron et al., 2004). In our initial experiments, large protruding clasts distorted velocity profiles while challenges in precise ADV placement meant that many sampling positions lay outside the inner 20 percent of depth where log-law conditions are most defensible (Afzalimehr and Anctil, 1999). As ADVs measure only a single point at a time, it can take many minutes to hours to obtain several profiles across a section. Within this time, the bed may change (aggrade or erode) under mobile conditions, creating discontinuities between ADV measurements at different locations. Moreover, the lack of suspended sediment in the water column resulted in insufficient seeding for acoustic reflection, limiting data quality. For future experiments, especially in the case of increasing sediment mobility, non-intrusive techniques should be explored such as Laser Doppler Velocimetry (LDV) and Large-Scale Particle-Image Velocimetry (LSPIV).

We also encountered challenges with uncertainty in drone-based topographic surveys due to the use of multiple DJI drone models (Mavic 2 Pro and Mini 2). Variations in camera specifications, lens distortion, flight stability, and image processing precision affected Digital Elevation Model (DEM) consistency—especially in overlapping zones or under low-light and windy conditions.

Environmental factors introduced additional complications. The growth of filamentous algae during the experiments interfered with sensor performance and could have altered channel hydraulics modifying sediment dynamics. This necessitated frequent manual cleaning of algae, the setup of temporary filtration systems, and the formulation of a broader water quality management plan. Research in the OERF also entails operational challenges inherent to outdoor facilities. For example, runoff from heavy rainfall can erode channel banks where flow spills off the floodplain, and birds and other wildlife may find the facility an attractive habitat. These complexities illustrate the challenges involved in maintaining consistent boundary conditions across multi-day experiments under semi-natural conditions.

https://doi.org/10.5194/egusphere-2025-4352
Preprint. Discussion started: 18 September 2025

5 Conclusions

In this contribution, we introduced the Outdoor Experimental River Facility (OERF) at the Université de Sherbrooke, Quebec, Canada, and quantified its operating envelope relative to natural rivers and existing indoor and outdoor river laboratories. We also reported results of an initial set of experiments with a straight–channel planform and staged bar–pool perturbation to explore thresholds of bank erosion and lateral migration. Within the feasible design space, flow in the OERF's 3 m wide gravel bedded channel was subcritical and fully rough at field–like Reynolds numbers ($\mathcal{O}(10^5)$). Under constant discharge without upstream sediment supply, the bed rapidly armoured (surface D_{50} from ~ 10 to ~ 22 mm), and reach–scale planform change remained limited over 338 h run time. The bar-pool perturbation increased local velocities (by 8–27 %) and concentrated shear stress along the outer bank, producing measurable but spatially confined bank retreat. Log–law shear stress estimates yielded median τ_0 of ~ 10, 16, 29, and 20 Pa across perturbation phases 0–3, exceeding phase–reference τ_c after Phase 1. Together, these results demonstrate that experiments in the OERF can reproduce field–like hydraulics and illustrate the difficulty of catalyzing planform evolution at scale under sediment–limited conditions.

Our initial experiments also provide lessons for future researchers designing outdoor experiments at this scale, including: (i) adding controlled sediment recirculation, extending run durations, and tuning slope, sediment grain size distributions (GSDs), and width–depth combinations to increase rates of morphological change; (ii) improve boundary controls through inlet flow–straightening/diffusion and tail–gate regulation; (iii) develop non-intrusive velocity measurements; and (iv) balance stronger bank-erosion drivers with additional bank strength such as floodplain vegetation to remain within the meandering domain ($W/D \lesssim 50$). Finally, although the staged bar-pool perturbation produced only local effects within the available experimental run time, testing hypotheses regarding the influence of perturbation type, magnitude, and timing on the onset and maintenance of meander bend growth remains a promising research opportunity for future experiments at the OERF.

Code and data availability. All datasets supporting this study is deposited in the Université de Sherbrooke Dataverse (Borealis) under the collection "GREAUS – Outdoor Experimental River Facility (OERF) / Données expérimentales" and made openly available at https://doi.org/10.5683/SP3/4VX2YI.

Author contributions. All authors (BM, ED, AR, MT, PB, LS, JL) contributed to the conceptualization, design, and execution of the experiments. ED led the design of the channel geometry and initial experiments. BM led the bar-pool perturbation design. AR contributed numerical simulations that informed the armouring analysis. BM, ED, and AR acquired and analyzed experimental data. BM prepared the original manuscript draft and led editing. All authors reviewed and revised the manuscript and approved the final version.

Competing interests. The authors declare that they have no conflict of interest.

https://doi.org/10.5194/egusphere-2025-4352
Preprint. Discussion started: 18 September 2025

Acknowledgements. This work was supported by the Fonds de recherche du Québec – Nature et technologies (FRQNT) (Team Research Project - 285933), and the Natural Sciences and Engineering Research Council of Canada (RGPIN-2019-05501; RGPIN-2023-05495). The construction of the Research Complex for Hydrology, Hydraulics, and the Environment of the Université de Sherbrooke which includes the OERF was supported by the Canadian Government's Post-Secondary Institutions Strategic Investment Fund, the Québec Government, the University of Sherbrooke, the UdeS Foundation, and several private donors and municipal partners: MRC de Memphrémagog, MRC Brome-Missisquoi, MRC du Granit, MRC du Val-Saint-François, and the City of Granby. We thank the Groupe de Recherche sur l'Eau de l'Université de Sherbrooke (GREAUS) for financial, logistical and technical support. We are grateful to the laboratory technicians Nicolas Simard and Daniel Breton for their assistance with OERF operations, instrumentation, and data collection.

https://doi.org/10.5194/egusphere-2025-4352
Preprint. Discussion started: 18 September 2025

References

Afzalimehr, H. and Anctil, F.: Velocity distribution and shear velocity behaviour of decelerating flows over a gravel bed, Canadian Journal of Civil Engineering, 26, 468–475, 1999.

Ashworth, P., Peakall, J., and Best, J.: Physical Modelling in Fluvial Geomorphology: Principles, Applications and Unresolved Issues, pp. 221–253, 1996.

Biron, P. M., Robson, C., Lapointe, M. F., and Gaskin, S. J.: Comparing different methods of bed shear stress estimates in simple and complex flow fields, Earth Surface Processes and Landforms: The Journal of the British Geomorphological Research Group, 29, 1403–1415, 2004.

Borsje, B., Kranenburg, W., Roos, P., Matthieu, J., and Hulscher, S.: The role of suspended load transport in the occurrence of tidal sand waves, Journal of Geophysical Research: Earth Surface, 119, 701–716, 2014.

Braudrick, C. A., Dietrich, W. E., Leverich, G. T., and Sklar, L. S.: Experimental evidence for the conditions necessary to sustain meandering in coarse-bedded rivers, Proceedings of the National Academy of Sciences, 106, 16 936–16 941, 2009.

Buffington, J. M. and Montgomery, D. R.: A systematic analysis of eight decades of incipient motion studies, with special reference to gravel-bedded rivers, Water resources research, 33, 1993–2029, 1997.

Bunte, K. and Abt, S. R.: Sampling surface and subsurface particle-size distributions in wadable gravel-and cobble-bed streams for analyses in sediment transport, hydraulics, and streambed monitoring, US Department of Agriculture, Forest Service, Rocky Mountain Research Station, 2001.

Chin, C., Melville, B., and Raudkivi, A.: Streambed armoring, Journal of Hydraulic Engineering, 120, 899–918, 1994.

Church, M. and Ferguson, R.: Morphodynamics: Rivers beyond steady state, Water Resources Research, 51, 1883–1897, 2015.

Coulthard, T. J. and Van De Wiel, M. J.: Modelling river history and evolution, Philosophical Transactions of the Royal Society A: Mathematical, Physical and Engineering Sciences, 370, 2123–2142, 2012.

Crosato, A. and Mosselman, E.: An integrated review of river bars for engineering, management and transdisciplinary research, Water, 12, 596, 2020.

Dey, S.: Fluvial hydrodynamics, Springer, 2014.

Dickson, E.: Characterization and prediction of fluvial bank retreat using novel physical experiments, Degree of master of science (geography, urban and environmental studies), Concordia University, 2023.

Dietrich, W. E., Kirchner, J. W., Ikeda, H., and Iseya, F.: Sediment supply and the development of the coarse surface layer in gravel-bedded rivers, Nature, 340, 215–217, 1989.

Eidmann, J. S. and Gallen, S.: New remote method to systematically extract bedrock channel width of small catchments across large spatial scales using high-resolution digital elevation models, Earth Surface Processes and Landforms, 48, 1470–1483, 2023.

Elgueta-Astaburuaga, M. A. and Hassan, M. A.: Experiment on temporal variation of bed load transport in response to changes in sediment supply in streams, Water Resources Research, 53, 763–778, 2017.

Felder, S. and Chanson, H.: Turbulence, dynamic similarity and scale effects in high-velocity free-surface flows above a stepped chute, Experiments in Fluids, 47, 1–18, 2009.

Ferguson, R. and Church, M.: A simple universal equation for grain settling velocity, Journal of sedimentary Research, 74, 933–937, 2004.

Folk, R. L. and Ward, W. C.: Brazos River bar [Texas]; a study in the significance of grain size parameters, Journal of sedimentary research, 27, 3–26, 1957.

Fredsøe, J.: Meandering and braiding of rivers, Journal of Fluid Mechanics, 84, 609–624, 1978.

https://doi.org/10.5194/egusphere-2025-4352
Preprint. Discussion started: 18 September 2025

Han, E. J., Kim, Y. D., Baek, K. O., and Seo, I. W.: Relation between transverse dispersion and diffusion at meandering channel in two-dimensional mixing based on tracer tests, Environmental Earth Sciences, 78, 1–11, 2019.

Kakinuma, T. and Shimizu, Y.: Large-scale experiment and numerical modeling of a riverine levee breach, Journal of Hydraulic Engineering, 140, 04014 039, 2014.

Khosronejad, A., Kozarek, J. L., and Sotiropoulos, F.: Simulation-based approach for stream restoration structure design: Model development and validation, Journal of Hydraulic Engineering, 140, 04014 042, 2014.

KICT: River Experiment Center (Andong), https://www.kict.re.kr/menu.es?mid=a20302030000, last access: 20 November 2023, 2023.

Knighton, D.: Fluvial forms and processes: a new perspective, Routledge, 2014.

Métivier, F., Lajeunesse, E., and Devauchelle, O.: Laboratory rivers: Lacey's law, threshold theory, and channel stability, Earth Surface Dynamics, 5, 187–198, 2017.

Métivier, F., Paola, C., Kozarek, J., and Tal, M.: Experimental studies and practical challenges in fluvial geomorphology, Tools in Fluvial Geomorphology, Second Edition., pp. 454–475, Wiley Online Library, ISBN 9780470684054, https://doi.org/10.1002/9781118648551.ch20, 2016.

Nelson, P. A., Dietrich, W. E., and Venditti, J. G.: Bed topography and the development of forced bed surface patches, Journal of Geophysical Research: Earth Surface, 115, 2010.

Papanicolaou, A. T. N., Elhakeem, M., Krallis, G., Prakash, S., and Edinger, J.: Sediment Transport Modeling Review—Current and Future Developments, Journal of Hydraulic Engineering, 134, 1–14, https://doi.org/10.1061/(ASCE)0733-9429(2008)134:1(1), 2008.

Parker, G., Toro-Escobar, C. M., Ramey, M., and Beck, S.: Effect of floodwater extraction on mountain stream morphology, Journal of Hydraulic Engineering, 129, 885–895, 2003.

Peakall, J., Ashworth, P. J., and Best, J. L.: Meander-Bend Evolution, Alluvial Architecture, and the Role of Cohesion in Sinuous River Channels: A Flume Study, Journal of Sedimentary Research, 77, 197–212, https://doi.org/10.2110/jsr.2007.017, 2007.

Phillips, C. B., Masteller, C. C., Slater, L. J., Dunne, K. B., Francalanci, S., Lanzoni, S., Merritts, D. J., Lajeunesse, E., and Jerolmack, D. J.: Threshold constraints on the size, shape and stability of alluvial rivers, Nature Reviews Earth & Environment, 3, 406–419, 2022.

PWRI-NRDA: Aqua Research Restoration Center, https://www.pwri.go.jp/team/kyousei/eng/about/m2_02%20facility_outline.htm, accessed on November 21, 2023, 2023.

Rachelly, C., Vetsch, D. F., Boes, R. M., and Weitbrecht, V.: Sediment supply control on morphodynamic processes in gravel-bed river widenings, Earth Surface Processes and Landforms, 47, 3415–3434, 2022.

Redolfi, M., Welber, M., Carlin, M., Tubino, M., and Bertoldi, W.: Morphometric properties of alternate bars and water discharge: a laboratory investigation, Earth Surface Dynamics, 8, 789–808, 2020.

Renault, A.: Modélisation numérique de la formation d'une couche de pavage dans une rivière expérimentale novatrice, Degree of master of science, Université de Sherbrooke, QC, 2024.

Rhoads, B. L.: River dynamics: geomorphology to support management, Cambridge University Press, 2020.

Rhoads, B. L. and Welford, M. R.: Initiation of river meandering, Progress in Physical Geography, 15, 127–156, 1991.

Rodríguez, E., Durand, M., and Frasson, R. P. d. M.: Observing Rivers With Varying Spatial Scales, Water Resources Research, 56, e2019WR026 476, https://doi.org/https://doi.org/10.1029/2019WR026476, e2019WR026476 10.1029/2019WR026476, 2020.

Saadon, A., Abdullah, J., Muhammad, N., Ariffin, J., and Julien, P.: Predictive models for the estimation of riverbank erosion rates, Catena, 196, 104 917, 2021.

https://doi.org/10.5194/egusphere-2025-4352
Preprint. Discussion started: 18 September 2025

Schleiss, A. J.: The challenge of restoring dynamics by river engineering: where to find the truth about river flow-in the computer, in the lab or in the field?, in: 9th International conference on fluvial hydraulics River Flow 2018, 2018.

Siva Subramanian, S., Fan, X., Yunus, A., Van Asch, T., Scaringi, G., Xu, Q., Dai, L., Ishikawa, T., and Huang, R.: A sequentially coupled catchment-scale numerical model for snowmelt-induced soil slope instabilities, Journal of Geophysical Research: Earth Surface, 125, e2019JF005 468, 2020.

Siviglia, A. and Crosato, A.: Numerical modelling of river morphodynamics: Latest developments and remaining challenges, 2016.

Sklar, L. S.: Grain size in landscapes, Annual Review of Earth and Planetary Sciences, 52, 663–692, 2024.

Smith, L. C.: Rivers of power: how a natural force raised kingdoms, destroyed civilizations, and shapes our world, Penguin UK, 2020.

UMN-CSE: Outdoor StreamLab - Anthony Falls Laboratory, https://cse.umn.edu/safl/outdoor-streamlab, accessed on November 20, 2023, 2023.

Van Dijk, W. M., Van de Lageweg, W., and Kleinhans, M. G.: Experimental meandering river with chute cutoffs, Journal of Geophysical Research: Earth Surface, 117, 2012.

Wei, X. and Li, Z.: Applicative limitations of sediment transport on predictive modeling in geomorphology, Journal of Geographical Sciences, 14, 94–104, 2004.

Wilcock, P. R. and Crowe, J. C.: Surface-based transport model for mixed-size sediment, Journal of hydraulic engineering, 129, 120–128, 2003.

Wohl, E.: A world of rivers: environmental change on ten of the world's great rivers, University of Chicago Press, 2010.

Wohl, E.: Rivers in the Landscape, John Wiley & Sons, 2020.

Yassine, R., Cassan, L., Roux, H., Frysou, O., and Pérès, F.: Numerical modelling of the evolution of a river reach with a complex morphology to help define future sustainable restoration decisions, Earth Surface Dynamics, 11, 1199–1221, 2023.

Zhao, K., Coco, G., Gong, Z., Darby, S. E., Lanzoni, S., Xu, F., Zhang, K., and Townend, I.: A review on bank retreat: Mechanisms, observations, and modeling, Reviews of Geophysics, 60, e2021RG000 761, 2022.